



---

## Figures and figure supplements

Odor identity coding by distributed ensembles of neurons in the mouse olfactory cortex

**Benjamin Roland *et al***

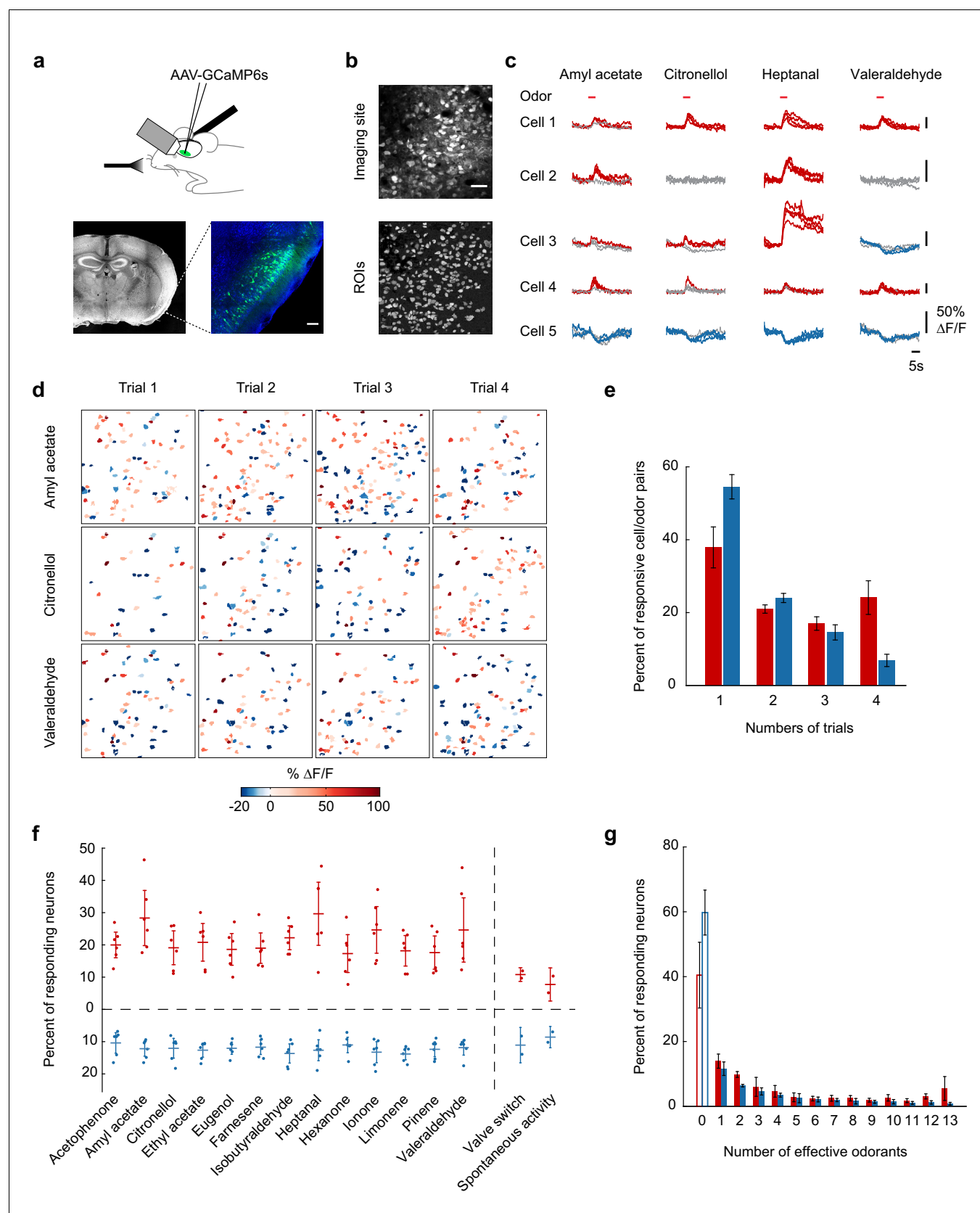


**Figure 1.** Calcium imaging of odor-evoked activity in piriform cortex. (a) (Top) Schematic of the experimental protocol. AAV-GCaMP6s was stereotactically injected into piriform cortex. After 10 days, piriform cortex was surgically exposed and neural activity in response to odors was recorded. Figure 1 continued on next page

*Figure 1 continued*

with two-photon imaging. (Bottom) Coronal section of a brain used for piriform imaging. Scale bar: 100  $\mu\text{m}$ . (b) (Top) Stack average of an imaging site, and (bottom) masks of the regions of interest (ROIs) identified by our clustering algorithm (see also **Figure 1—figure supplement 1**). Scale bar: 50  $\mu\text{m}$ . (c) Single-trial example traces of four different cells (rows) in response to four different monomolecular odorants (columns). Cells respond with an increase (red traces) or a decrease (blue traces) in fluorescence (gray traces: non responsive trials). Note the different scale of  $\Delta F/F$  values (y axis) for each neuron. Red bar: odor presentation. (d) Spatial patterns of piriform activity in response to four trials (columns) of three different monomolecular odorants (rows).  $\Delta F/F$  values are clipped at 100% here and henceforth in all figures. Odorants activate sparse, distributed, and partially overlapping ensembles of piriform neurons. (e) Reliability of activation (red) and suppression (blue), measured as the number of trials each cell-odor pair responded to a given odorant, averaged across imaging sites ( $n = 6$  sites in three mice). Error bars: 95% CI of the mean. (f) Percent of neurons activated (red) or suppressed (blue), averaged across four trials. Dots: single data points from individual imaging sites. Horizontal bars: mean across imaging sites ( $n = 6$ ). Error bars: 95% CI of the mean. (g) Tuning curve of activation (red) and suppression (blue), averaged across imaging sites ( $n = 6$ ). Error bars: 95% CI of the mean.

DOI: [10.7554/eLife.26337.002](https://doi.org/10.7554/eLife.26337.002)

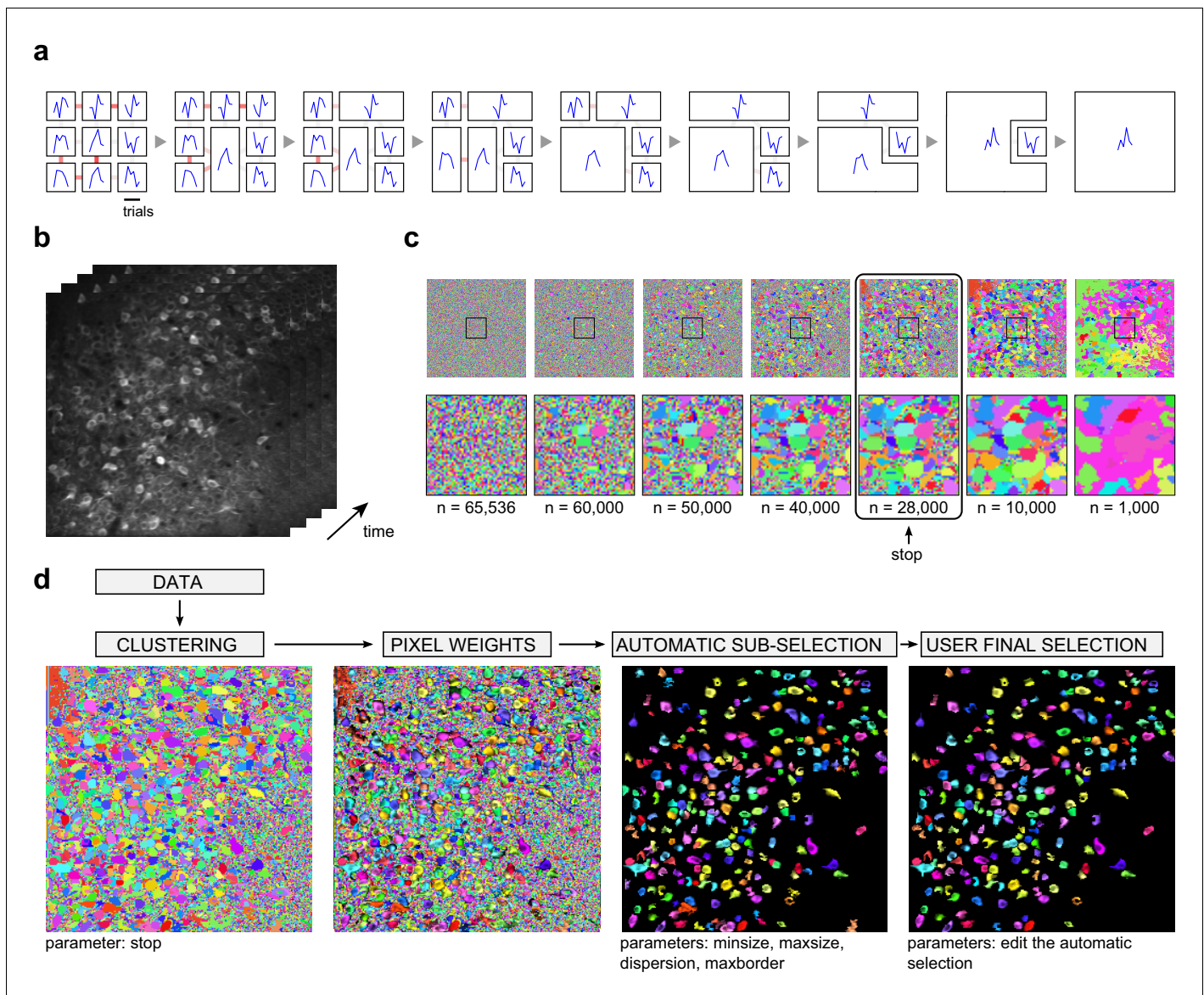


**Figure 1—figure supplement 1.** Automated cell segmentation. (a) Illustration of the clustering method on a schematic movie with 3 x 3 pixels and 6 frames. Left: each square represents a pixel; signals of individual pixels are shown and links between neighboring pixels are color-coded according to correlation values. Second from left: the pair of most correlated neighbors is merged into a single region, a new signal is attributed to this region by averaging the two original signals, and correlations with this new signal are updated. The process is then repeated until all initial pixels have been clustered into a single region. (b) Illustration on an experimental dataset, and representation of individual movie frames. (c) Different stages of the clustering are shown, from individual pixels in the 256 x 256 image to 1000 clustered regions. The bottom row magnifies the region indicated with a square in the top row. Pixels from the most active neurons are the first to cluster. A 'stop' parameter determines when the clustering should be interrupted (typically, before individual neurons start to merge, or merged with the neuropil region). (d) In addition to the clustering, the segmentation procedure includes the computation of individual pixel contributions (weights) to each region, an automatic sub-selection of regions that have typical neuronal size and shape, and a manual validation of the sub-selection (see Materials and methods for details).

DOI: [10.7554/eLife.26337.003](https://doi.org/10.7554/eLife.26337.003)

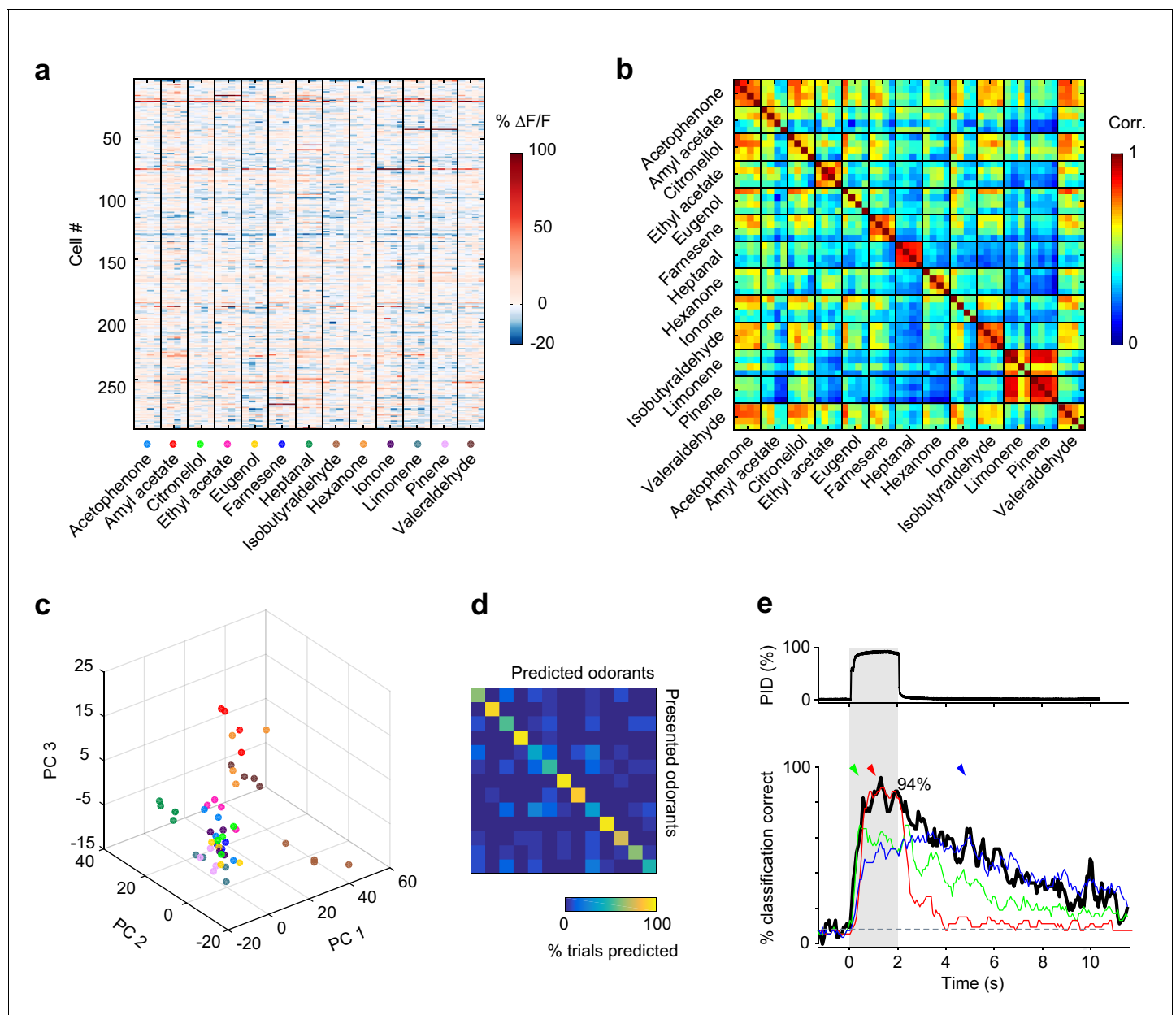


**Figure 2.** Odor identity is encoded in the spatial patterns of piriform activity. (a) Population response of the imaging site shown in **Figure 1a**. The mean  $\Delta F/F$  value after stimulus onset for each trial (columns) in each cell (rows) is color-coded. (b) Similarity matrix obtained by computing the pairwise correlation coefficients between all population response vectors in (a). Squares along the diagonal ( $4 \times 4$  trials) represent the similarity of responses to four exposures of the same odorant (intra-stimulus cross-trial correlations). (c) Patterns of piriform activity in response to single odor presentations (dots represent different odorants, color-coded as in (a)) projected onto space of the first three principal components (accounting for ~20% of the total variance). Neurons were pooled across imaging sites. (d) Confusion matrix summarizing the performance of a linear classifier trained to discriminate the odorants in A, summed over imaging sites ( $n = 6$  sites in three mice). (e) Percent of trials correctly identified by a linear classifier, for neurons pooled across all six imaging sites (blackline). Green, red and blue lines represent classification accuracy obtained with a classifier trained on response patterns at 0.27 (green arrowhead), 1 (red arrowhead) and 3 (blue arrowhead) s after odor onset. Gray dashed line: theoretical chance level. Gray square: odor exposure.

DOI: [10.7554/eLife.26337.004](https://doi.org/10.7554/eLife.26337.004)

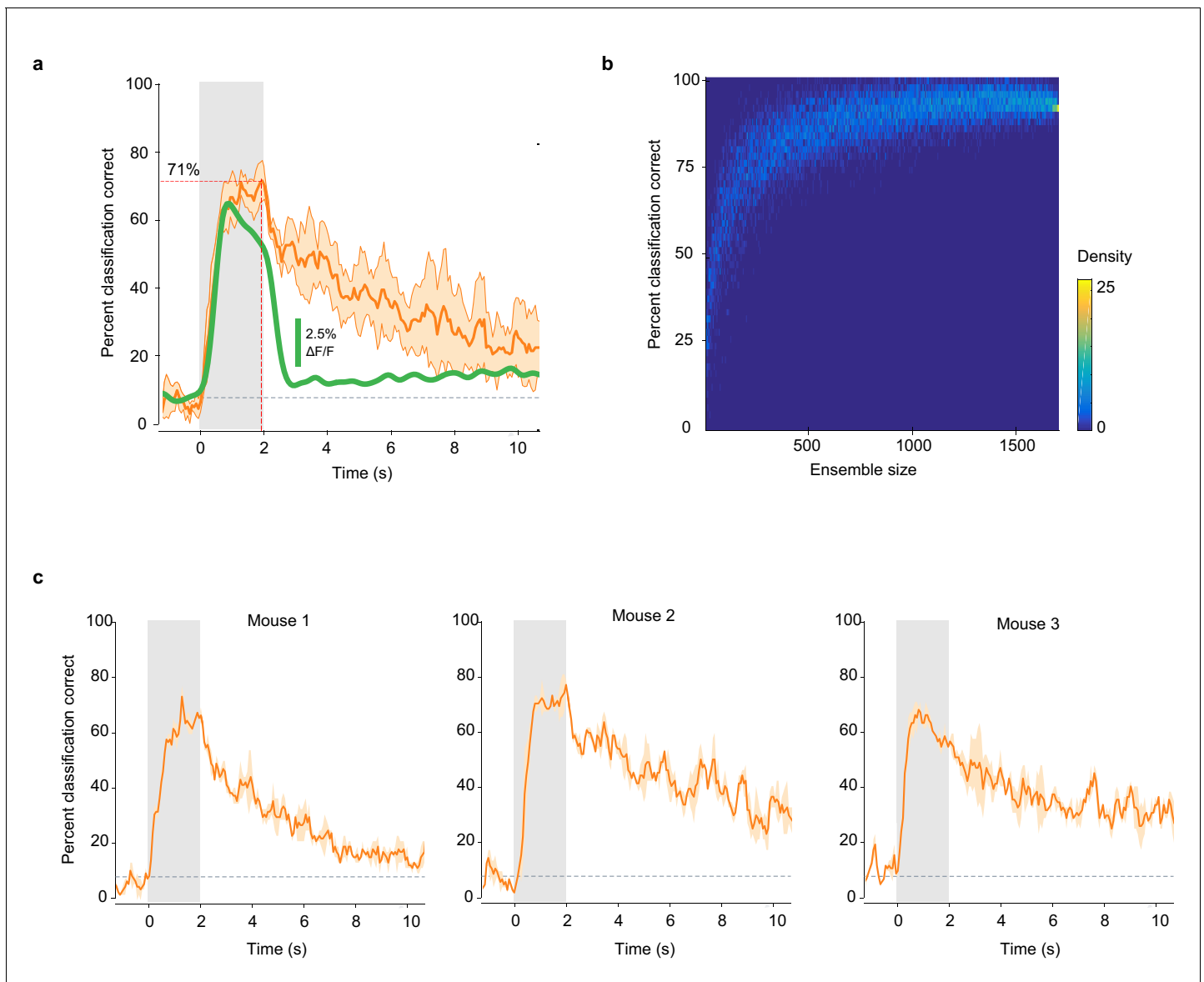


**Figure 2—figure supplement 1.** Classification accuracy is consistent across mice and imaging sites. (a) Percent of trials correctly identified by a linear classifier, averaged across six imaging sites (orange line). Shaded area: SD of the mean. Green line: mean deconvolved  $\Delta F/F$  values of significant odor-evoked responses. Gray square: odor exposure. (b) Accuracy of odor identity classification in pseudo-populations of increasing size. Distribution of the accuracy of odor classification by a linear classifier trained on pseudo-populations of piriform ensembles ( $n = 10,000$ ) of increasing size, randomly sampled from the dataset presented in **Figure 2** (1703 neurons in three mice). (c) Classification accuracy is highly consistent across mice. Percent of trials correctly identified by a linear classifier, averaged within each mouse of the dataset used in **Figure 2**. Shaded area: SD of the mean. Gray squares: odor exposure.

DOI: [10.7554/eLife.26337.005](https://doi.org/10.7554/eLife.26337.005)

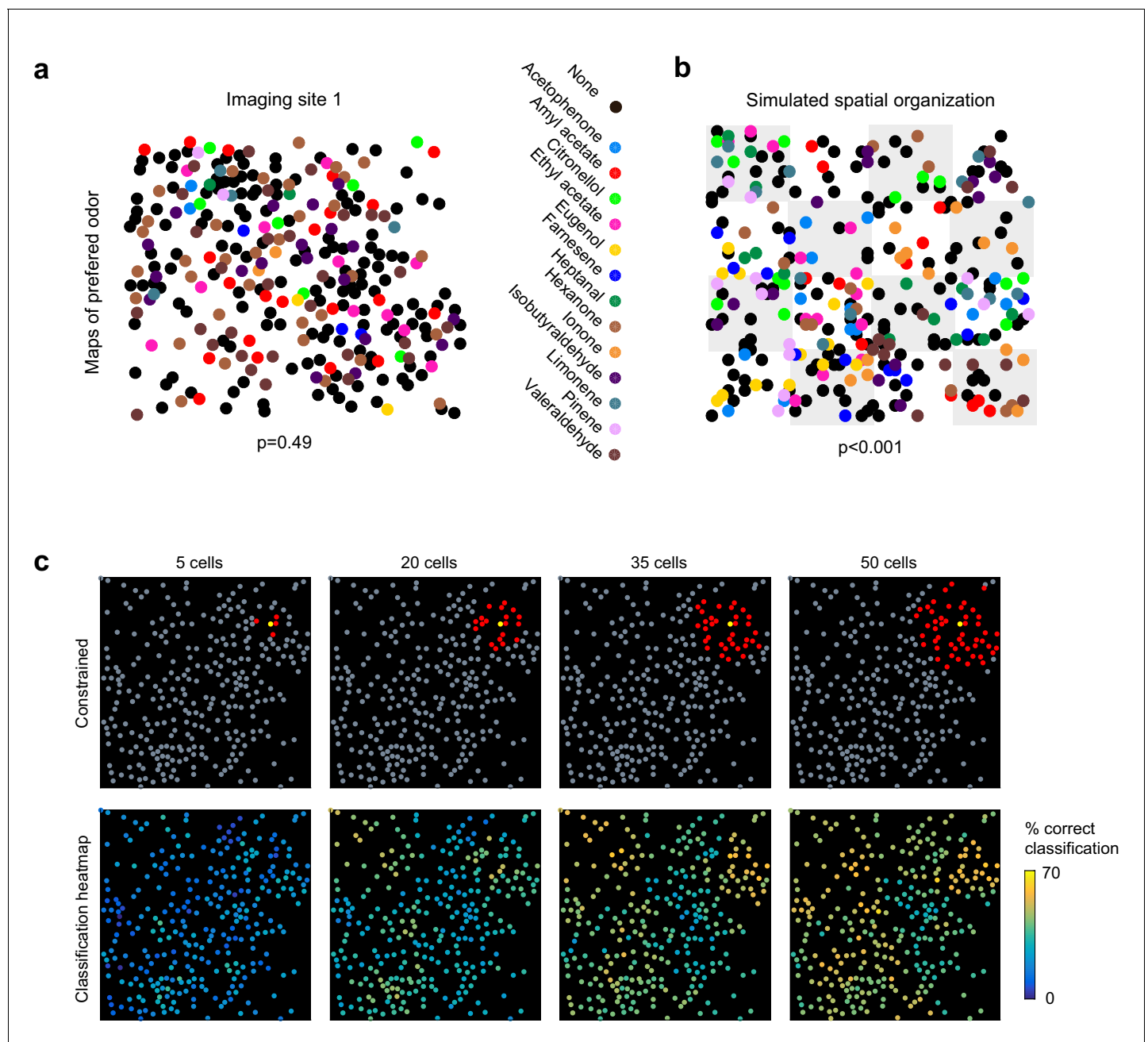


**Figure 3.** No evidence for topography in patterns of piriform activity. (a) Odorant preference map for an imaging site, with the odorant preference of individual piriform neurons color coded as in **Figure 2**. (b) Example of simulated clustering. The imaging site was divided into 16 equally sized sub-areas and preference for an odorant was allowed to occur in only three or four randomly chosen sub-areas. The p value indicates the probability that the computed nearest neighbor index is different from randomly distributed neurons. (c) (Top) Example of an ensemble of piriform neurons (in red) locally constrained around a 'starter cell' (in yellow), and used for classification of the stimulus set of **Figure 2**. (Bottom) Heatmaps of the classification accuracy of different starter cells for piriform ensembles of increasing size.

DOI: [10.7554/eLife.26337.006](https://doi.org/10.7554/eLife.26337.006)



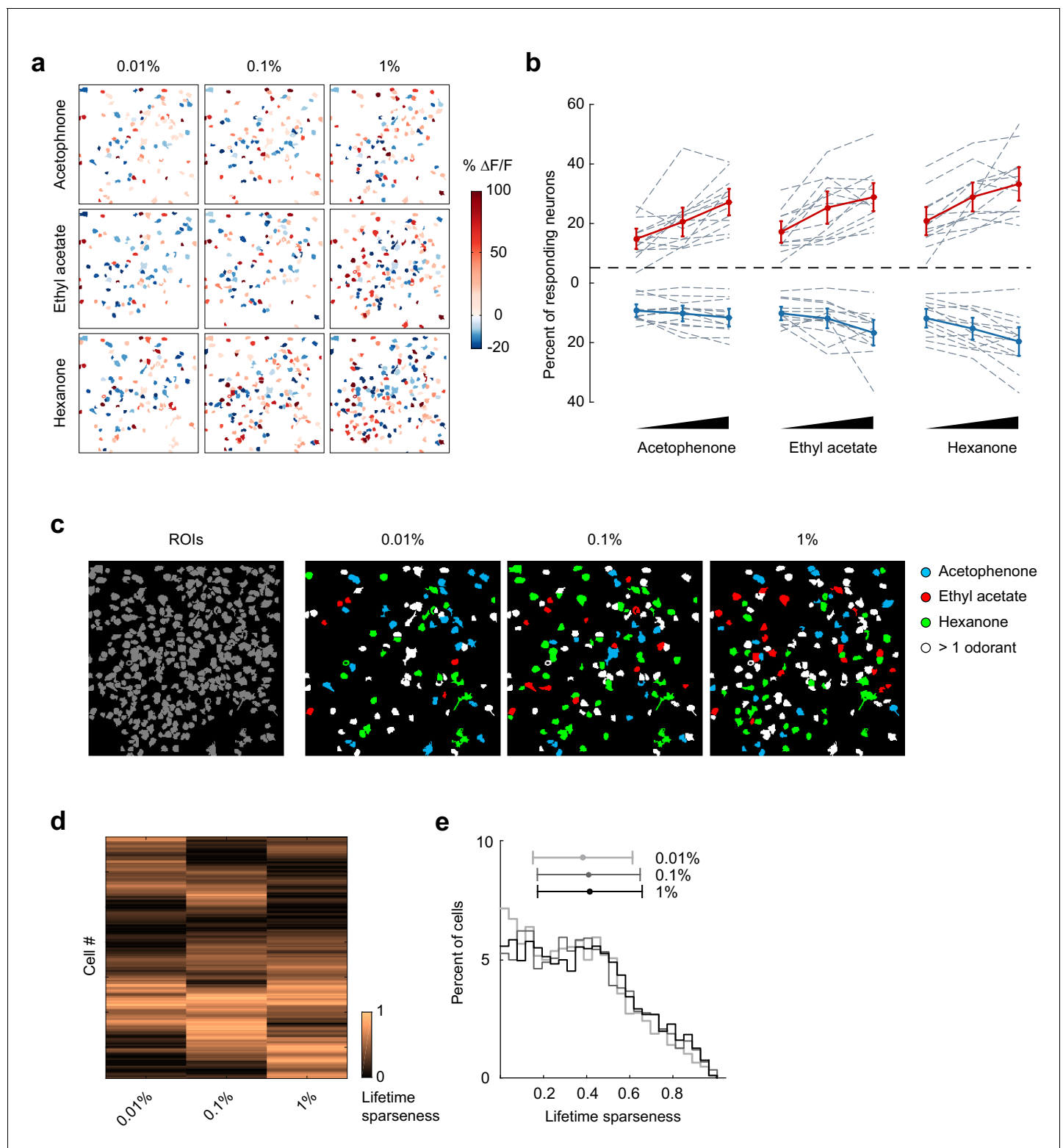


**Figure 4.** Odor-evoked activity and sparseness of individual piriform neurons depends on odorant concentration. (a) Spatial patterns of piriform activity in response to acetophenone, ethyl acetate and hexanone at three different concentrations (1:10,000, 1:1,000, 1:100 vol./vol. dilutions). (b) Percent of neurons activated or suppressed by acetophenone, ethyl acetate, and hexanone at three different concentrations (1:10,000, 1:1,000, 1:100 vol./vol. dilutions). Dashed gray lines represent individual imaging sites, thick red (activation) and blue (suppression) lines represent averages across sites ( $n = 13$  sites in 11 mice). Error bars: 95% CI of the mean. (c) Spatial patterns of piriform activity in response to acetophenone, ethyl acetate and hexanone at Figure 4 continued on next page



*Figure 4 continued*

three different concentrations (1:10,000, 1:1,000, 1:100 vol./vol. dilutions). Only cells responding at least two out of four trials are depicted. Cells responding to multiple odorants are color-coded in white. **(d)** Matrix of lifetime sparseness across concentrations for the cells in **(c)**, sorted by hierarchical clustering. **(e)** Distribution of lifetime sparseness of all neurons pooled across imaging sites ( $n = 13$ , total number of neurons = 2935). DOI: [10.7554/eLife.26337.007](https://doi.org/10.7554/eLife.26337.007)

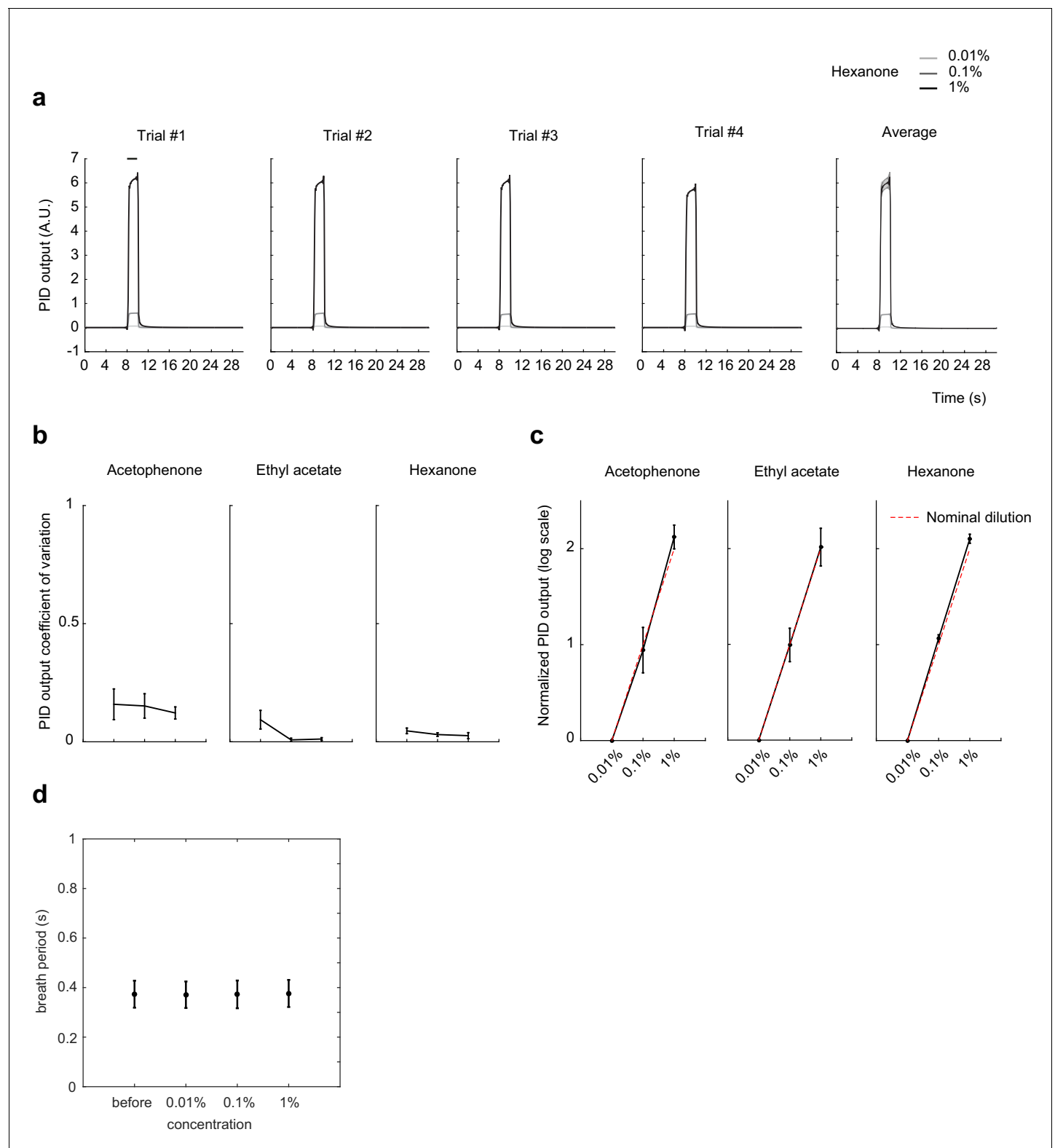


**Figure 4—figure supplement 1.** Odorant concentration scales with nominal dilution and breath period is independent of odorant concentration. (a) Photoionization detector (PID) traces for Hexanone at 1:10,000, 1:1,000, and 1:100 vol./vol. dilution in mineral oil. Four individual trials and average trace across the four trials are shown. Shaded area: SD of the mean. (b) Coefficient of variation of the mean PID signal after odor onset, averaged across 14 trials. Error bar: SD of the mean. (c) Mean PID signal normalized to 1:10,000 vol./vol. dilution, averaged across 14 trials. Red dotted line shows the nominal dilution. (d) Mean PID signal normalized to 1:10,000 vol./vol. dilution, averaged across 14 trials. *Figure 4—figure supplement 1 continued on next page*

Figure 4—figure supplement 1 continued

expected output from nominal dilutions. Error bar: SD of the mean. (d) Breath period of mice before and after exposure to odorants at different concentrations. Error bar: SD of the mean.

DOI: [10.7554/eLife.26337.008](https://doi.org/10.7554/eLife.26337.008)

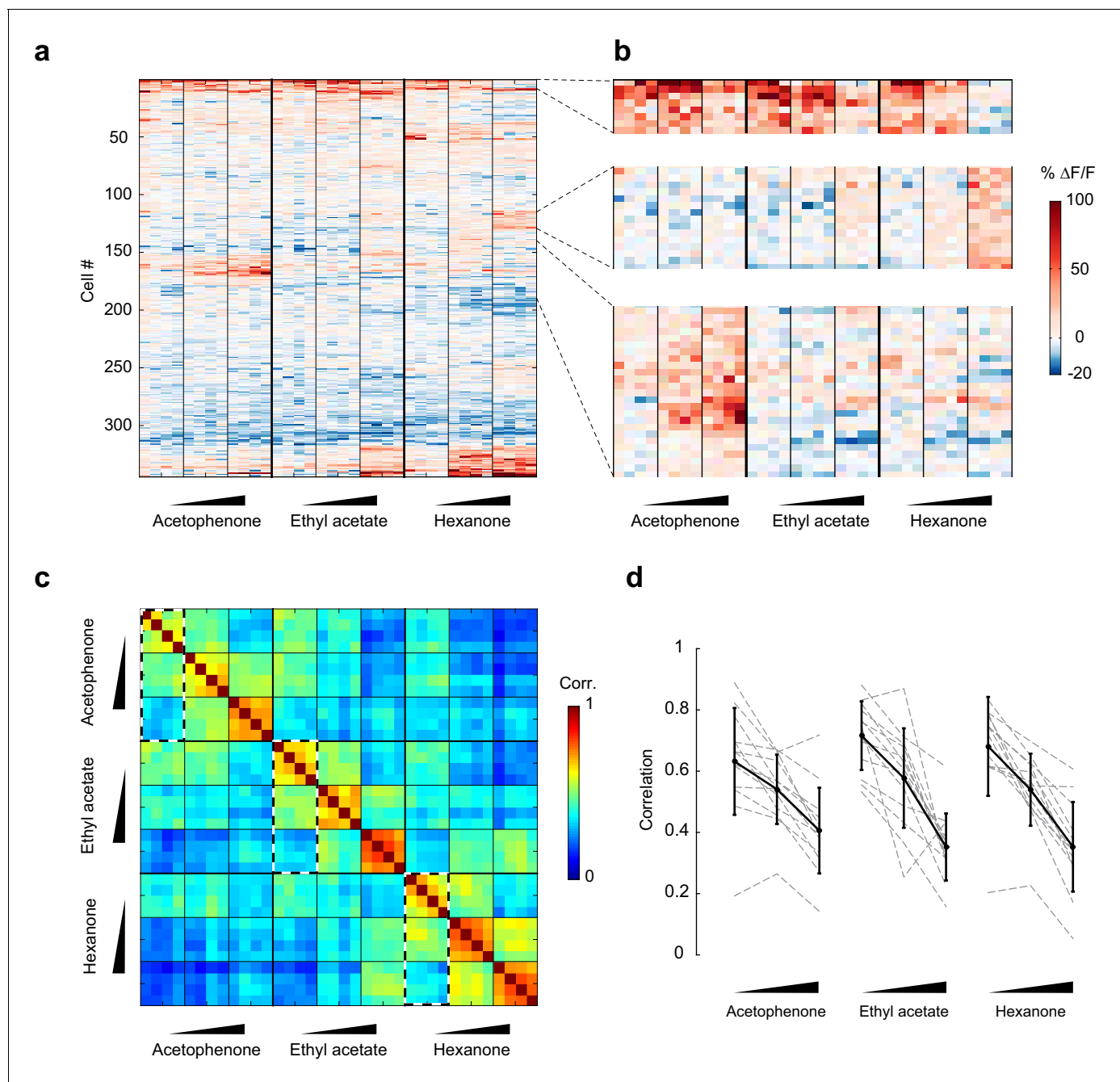


**Figure 5.** Patterns of piriform activity decorrelate with increasing odorant concentrations. **(a)** Population response of the imaging site in **Figure 3a** to acetophenone, ethyl acetate and hexanone at three different concentrations (1:10,000, 1:1,000, 1:100 vol./vol. dilutions). Cells are sorted by hierarchical clustering. **(b)** Example response profiles of cells suppressed at higher concentrations for all three odorants (top panel), cells moderately enhanced by increasing concentrations of ethyl acetate or hexanone (middle panel), and cells strongly enhanced by increasing concentrations of acetophenone (bottom). **(c)** Similarity matrix obtained by computing the pairwise correlation coefficients between all response vectors pooled across imaging sites. Squares along the diagonal ( $4 \times 4$  trials) represent the similarities of responses to a single odorant/concentration pair (intra-stimulus cross-trial correlations). Large squares ( $12 \times 12$  trials) represent the similarities of responses to an odorant at varying concentrations (intra-odorant cross-trial correlations). The similarities of responses to increasing concentrations of a given odorant (intra-odorant inter-concentrations similarity) are highlighted by dashed line rectangles. **(d)** Correlation coefficients of the patterns of piriform activity elicited at increasing concentrations with the patterns elicited at low concentrations. Dashed gray lines represent individual imaging sites, thick black lines the average across sites ( $n = 13$  sites in 11 mice). Error bars: 95% CI of the mean. Patterns of piriform activity along increasing concentrations gradually decorrelate from the patterns elicited at low concentration.

DOI: [10.7554/eLife.26337.009](https://doi.org/10.7554/eLife.26337.009)

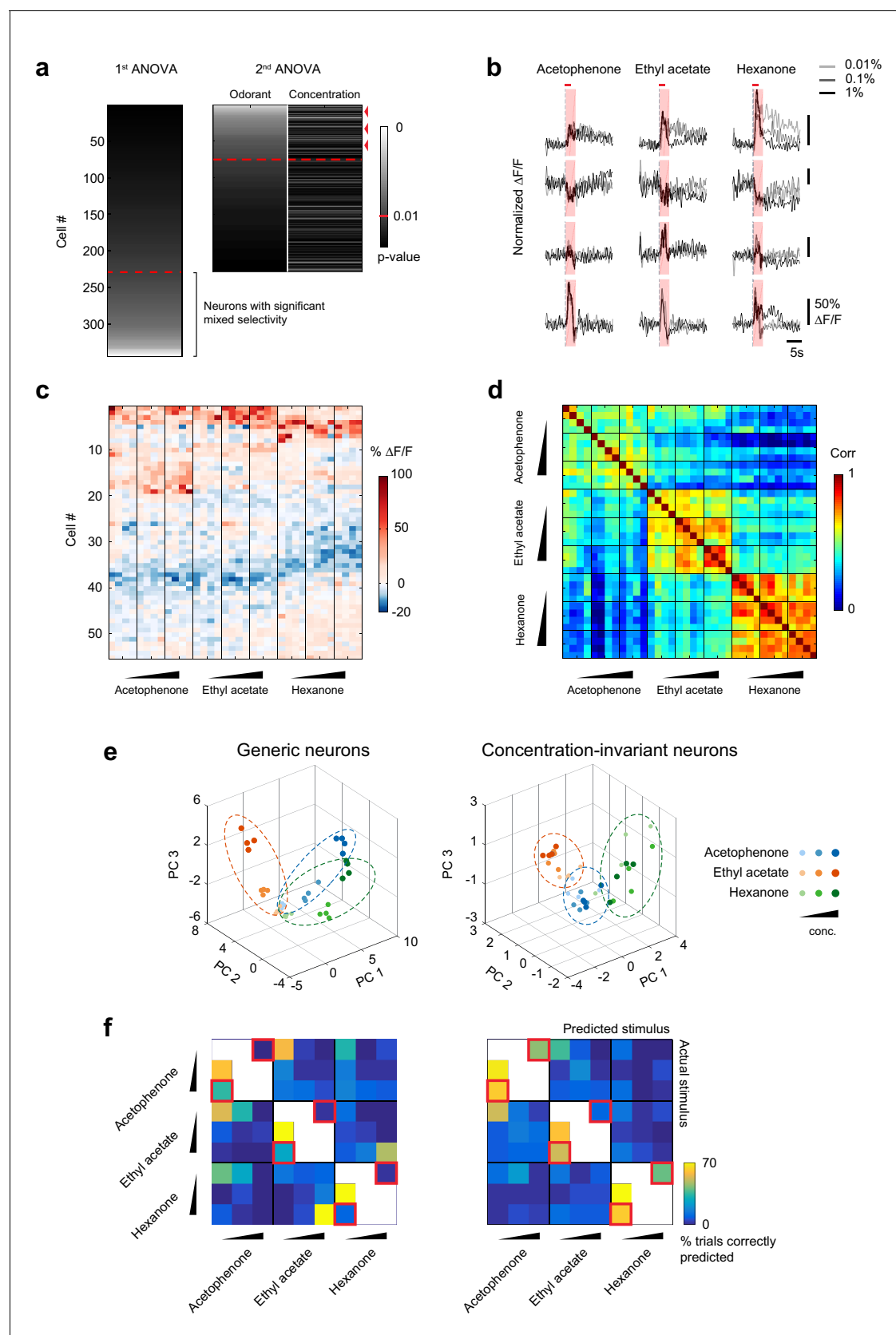


**Figure 6.** A concentration-invariant subnetwork of piriform neurons. (a) Summary of the analysis of variance of the response profiles of cells in **Figure 4a**. Two ANOVAs are performed successively. In the first step, neurons with mixed selectivity are excluded from the analysis. Concentration-

*Figure 6 continued on next page*

*Figure 6 continued*

invariant cells are then identified as cells significantly modulated by odorant identity but not concentration (red arrowheads: example cells). These cells are used for subsequent analyses against the population of all other 'generic neurons'. Red dashed line: significance threshold, set at  $p=0.01$ . (b) Deconvolved response traces of 4 concentration-invariant cells (rows) to acetophenone, ethyl acetate and hexanone at three different concentrations (light grey: 1:10,000, dark grey: 1:1,000, black 1:100 vol./vol. dilutions).  $\Delta F/F$  values are normalized to each cell's maximum  $\Delta F/F$ . Red bar: odor presentation. Shaded area: time interval used to integrate  $\Delta F/F$  values for the analysis of variance in (a). (c) Response matrix of the population of cells in (a) exclusively modulated by odorant identity.  $\Delta F/F$  values do not vary significantly with increasing odorant concentrations. (d) Similarity matrix obtained by computing the correlation coefficients between patterns of concentration-invariant neurons pooled across imaging sites ( $n = 13$ ). Responses of concentration-invariant neurons to different concentrations of a given odorant (intra-odorant inter-concentrations similarity) are as correlated as responses to the same odorant/concentration pair. (e) Patterns of activity of generic neurons (left) or concentration-invariant neurons (right) in response to single-odor presentations (dots) projected onto space of the first three principal components. Neurons were pooled across imaging sites ( $n = 13$ ). (f) Confusion matrix summarizing the accuracy of the classification of odorant identity by generic neurons (left) or concentration-invariant neurons (right) in a generalization task (see Materials and methods), summed over imaging sites ( $n = 13$ ). The classifier assigns each odor trial to one of seven stimulus groups. Two concentrations of the tested odorant (including the tested concentration) are excluded from the training data (white boxes). Difficult generalization tasks across a 100-fold change in odorant concentration are highlighted by the red squares.

DOI: [10.7554/eLife.26337.010](https://doi.org/10.7554/eLife.26337.010)

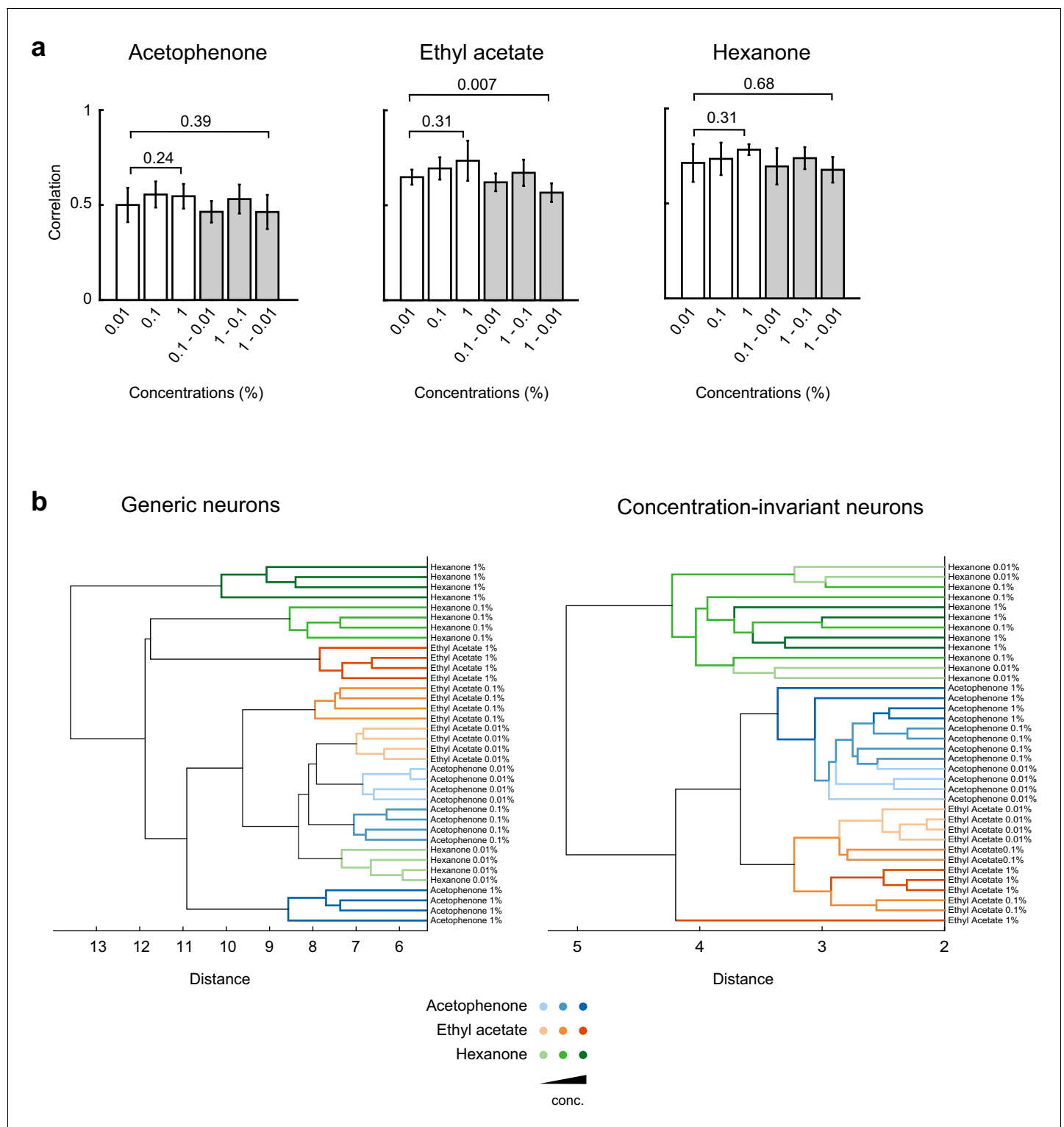


**Figure 6—figure supplement 1.** Cross-correlation and principal component analysis of concentration-invariant piriform neurons. (a) Correlation coefficients of odor-evoked responses of concentration-invariant piriform neurons. Cross-trial correlations at a given concentration (empty bars) did not significantly change across concentrations for all three odorants. Cross-trial correlations for acetophenone and hexanone responses at low concentration were not significantly different from the cross-concentration correlations for low versus high odorant concentrations. A small but significant difference was observed for cross-concentration correlations for ethyl acetate (cross-trial correlations at 0.01%:  $0.57 \pm 0.04\%$  SD, cross-concentration correlations 0.01 versus 1%:  $0.65 \pm 0.05\%$  SD,  $p=0.007$ ). (b) Hierarchical clustering of the data transformed into principal components

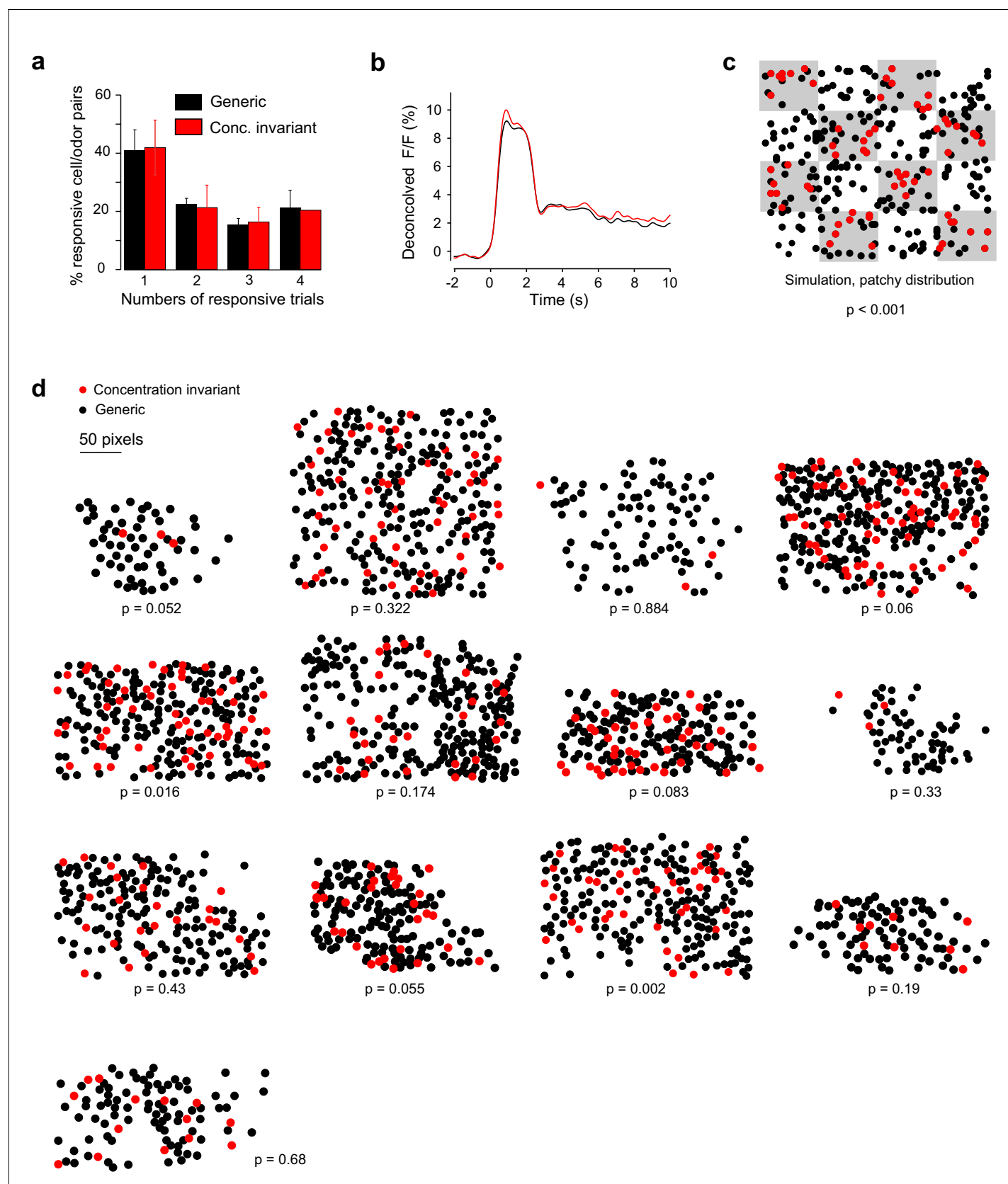
Figure 6—figure supplement 1 continued on next page



Figure 6—figure supplement 1 continued

(**Figure 6e**) shows that patterns of activity of generic neurons cluster systematically by concentration, but not by odorant identity. In contrast, patterns of concentration-invariant neurons cluster by odorant identity but do not systematically cluster by concentrations.

DOI: [10.7554/eLife.26337.011](https://doi.org/10.7554/eLife.26337.011)



**Figure 6—figure supplement 2.** Response properties and spatial organization of concentration-invariant piriform neurons. (a) Trial-to-trial variability, measured as the percentage of trials each cell-odor pair responded to a given odorant, for concentration-invariant and generic neurons, averaged Figure 6—figure supplement 2 continued on next page

*Figure 6—figure supplement 2 continued*

across imaging sites ( $n = 13$  sites in 11 mice). Error bars: 95% CI of the mean. **(b)** Odor-evoked change in fluorescence ( $DF/F$ ) for concentration-invariant and generic neurons. **(c)** Simulated clustering of concentration-invariant neurons. The imaging site was divided into 16 equally sized sub-areas and concentration-invariance was allowed to occur in half of the sub-areas. The p value indicates the probability that the computed nearest neighbor index for the concentration invariant neurons is different from randomly distributed neurons. **(d)** Spatial distribution of concentration-invariant neurons for each imaging site. The p value indicates that the probability with which the nearest neighbor index of the observed spatial distribution can be explained by a randomly distributed ensemble, simulated by cell identity shuffling.

DOI: [10.7554/eLife.26337.012](https://doi.org/10.7554/eLife.26337.012)

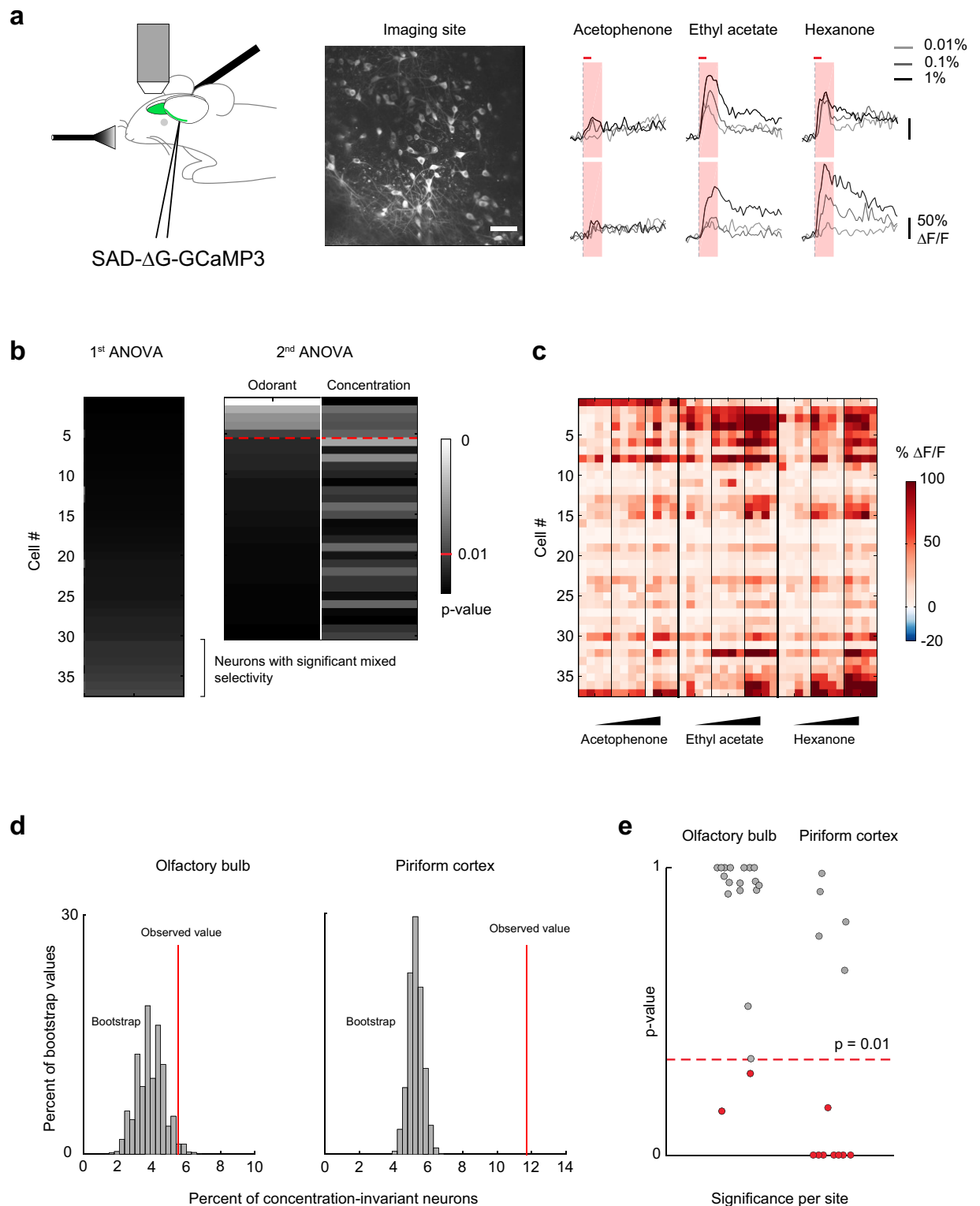


**Figure 7.** Concentration-invariant representations of odor identity emerge in the piriform cortex. (a) (left) Schematic of the experimental protocol. Rabies-GCaMP3 was injected underneath the lateral olfactory tract. After 5–7 days, the olfactory bulb was surgically exposed and mitral cell activity in response to odorants was recorded with two-photon imaging. (middle) Stack average of an imaging site. Scale bar: 50  $\mu\text{m}$ . (right) Deconvolved

*Figure 7 continued on next page*

*Figure 7 continued*

response traces of two neurons to acetophenone, ethyl acetate and hexanone at three different concentrations (light grey: 1:10,000, dark grey: 1:1,000, black 1:100 vol./vol. dilutions). Red bar: odor presentation. Shaded area: time interval used to integrate  $\Delta F/F$  values for the analysis of variance in (b). (b) Summary of the analysis of variance of the response profiles of a mitral and tufted cell imaging site. See also **Figure 5a**, and Materials and methods for details. (c) Population response of the imaging site in (a) to acetophenone, ethyl acetate and hexanone at three different concentrations (1:10,000, 1:1,000, 1:100 vol./vol. dilutions). Cells are sorted by the p-value of the effect of odorant identity. (d) Percent of concentration-invariant neurons (red line) identified in the olfactory bulb (left, n = 19 imaging sites in eight mice) and in piriform cortex (right, n = 13 imaging sites in 11 mice), overlaid onto the distribution of the percent of concentration-invariant neurons found in the bootstrap samples. (e) p-Values for the number of concentration-invariant neurons identified at each imaging site in the olfactory bulb (left, n = 19) and the piriform cortex (right, n = 13). The number of concentration-invariant neurons is significantly above chance (red dots,  $p < 0.01$ ) in 8 out of 13 imaging sites in the piriform cortex, but only in 2 out of 19 imaging sites in the olfactory bulb.

DOI: [10.7554/eLife.26337.013](https://doi.org/10.7554/eLife.26337.013)

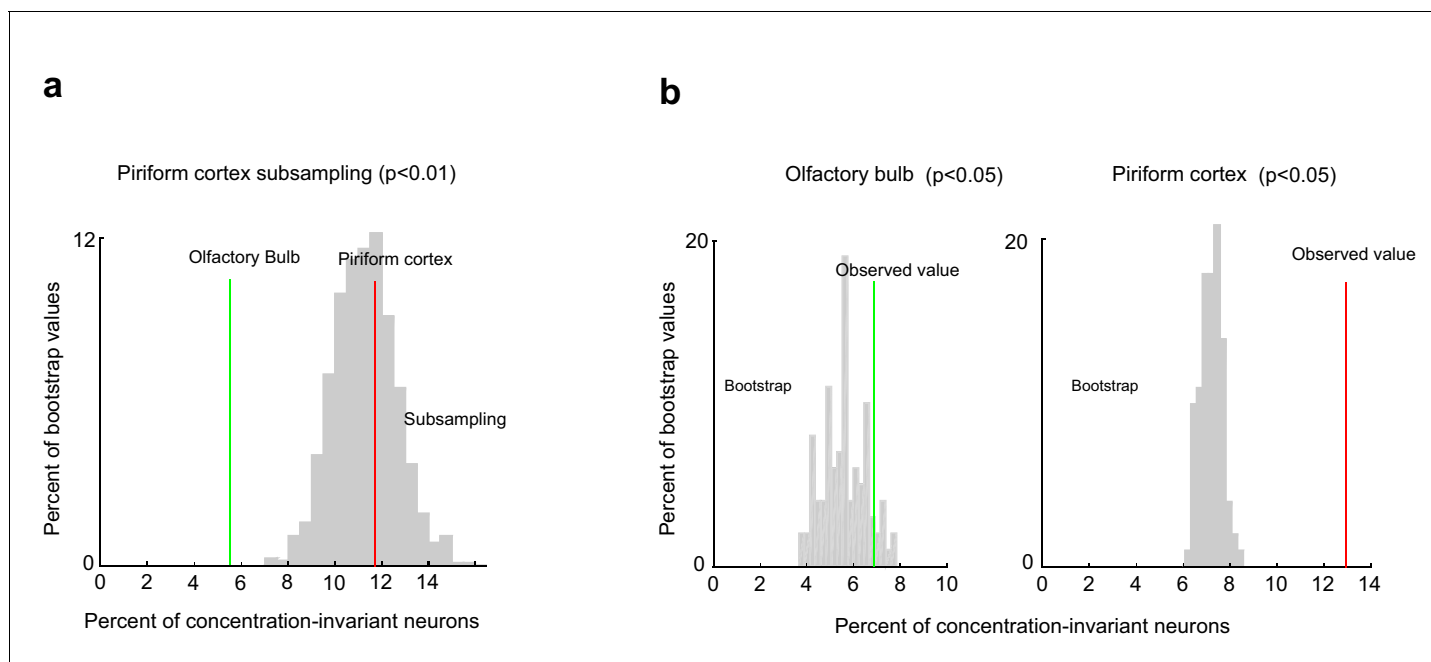


**Figure 7—figure supplement 1.** Comparison of the fraction of concentration-invariant neurons in piriform cortex and olfactory bulb. (a) Percent of concentration-invariant neurons identified in the olfactory bulb (green line) and in piriform cortex (red line), overlaid onto the distribution of the percent of concentration-invariant neurons found with 1000 random iterations of subsampling 500 piriform neurons (gray). (b) Percent of concentration-invariant neurons identified in the olfactory bulb (green line) and in piriform cortex (red line), overlaid onto the distribution of the percent of concentration-invariant neurons found in the bootstrap samples (gray). As in **Figure 7**, but with a significance criterion of  $p < 0.05$ .

DOI: [10.7554/eLife.26337.014](https://doi.org/10.7554/eLife.26337.014)